**UNITED STATES PATENT AND TRADEMARK OFFICE**

---

**BEFORE THE PATENT TRIAL AND APPEAL BOARD**

---

**Abiomed, Inc., Abiomed R&D, Inc., and Abiomed Europe GmbH**
***Petitioners***

**v.**

**Maquet Cardiovascular, LLC**
***Patent Owner***

---

**Case IPR2017-02151**
**U.S. Patent No. 9,327,068**

---

---

**PATENT OWNER'S EXHIBIT 2006**

---

*Artificial Organs*
20(6):650–661, Blackwell Science, Inc., Boston


# Hemodynamic System Analysis of Intraarterial Microaxial Pumps In Vitro and In Vivo

Thorsten Siess, *Bart Meyns, Klaus Spielvogel, Helmut Reul, Günter Rau, and *Willem Flameng

*Helmholtz Institute for Biomedical Engineering, Aachen University of Technology, Aachen, Germany; and *Centrum voor experimentele Heelkunde en Anesthesiologie, Leuven, Belgium*

**Abstract:** Because of the lack of a sophisticated pump management system, the performance of the Hemopump in patients cannot be assessed successfully. To clarify the interrelationship between an intravascular nonpulsatile pump and a pulsating ventricle, an in vitro study was set up under controlled conditions. Before these in vitro experiments, a series of in vivo experiments were performed in sheep using Hp31 cannulae. As anticipated, the resulting pulsatile pump flow was a function of the momentary pressure difference across the pump. This varying pump flow showed a significant flow loop hysteresis, indicating that the pressure difference across the pump is not the only parameter governing momentary pump flow of a rotary pump operating at constant speed in a pulsatile environment. Furthermore, flow in the Hp31 was significantly influenced by the inflow situation, blood supply, size of the ventricular cavity, and shape and position of the inflow cannula within the ventricle. Pulsatile flow conditions with good as well as impaired inflow into the pump were accordingly simulated in vitro to verify the in vivo measurements, to characterize the various inflow conditions, and to discuss methods of improved pump management. As a result of the in vivo and in vitro experiments, one can rely on the measurement of nonpulsatile in vitro flow and pressure differences across the pump to characterize the momentary pump flow for good inflow conditions into the pump. For these situations, the flow hysteresis produced, caused by fluid inertia within the pump and cannula, can be neglected. In contrast, for an impaired inflow situation, the calculated pump flow based on pressure difference measurements can be misleading. Consequently, an improved pump management system is required to adjust the pump speed, the pump performance, to any kind of impaired inflow. **Key Words:** Intravascular rotary blood pump—Pump-ventricle interaction—Pump management.

Based on the in vivo experience with the Hemopump cannulea (Medtronic, Minneapolis, Minnesota, U.S.A.) placed either transthoracically (Model Hp31) or inserted through the femoral artery (Models Hp21 and Hp14), the need for a more profound knowledge of the pump's performance in vivo has been discussed (1,2,3,4). Presently, these intravascular pumps run at a constant rotation speed and indicate "pump performance" on a panel of the driving console (5). This "performance" is based on the alternating motor current resulting from the changing pressure and flow conditions within the ventricle. Although this method is useful to ensure that the inflow tip of the cannula is positioned within the ventricle, it does not directly relate pump speed to a measured or calculated pump flow and thus is not a direct measure of actual pump performance and the perfusion of the patient. Consequently, a sophisticated online control of the Hemopump's performance is not available presently and also is difficult to integrate into the existing system. Proper patient management thus is difficult to achieve.

Initial animal experiments have been conducted to characterize pump performance in combination with a beating ventricle (2). These results must be validated in vitro and may lead to a more profound understanding of pump ventricular interaction and to a better system of pump management based on reliable online data from which the pump flow may be calculated and suction of the inflow cannula to the myocardium may be avoided.

Received January 1996.
Address correspondence and reprint requests to Dr. T. Siess at Helmholtz Institute for Biomedical Engineering, Aachen University of Technology, Pauwelsstrasse 20, D-52074 Aachen, Germany.

The results of this study are important for the development of the Helmholtz intravascular microaxial pump (6,7) and may be applied directly to this new system. As a result of these studies and in conjunction with the development of suitable insertion techniques, a complete pump system consisting of pump and proximal motor unit, an inflow catheter, and a guiding catheter is under development at the Helmholtz Institute. A reasonable pump management system based on online pump flow information will be incorporated.

## MATERIAL AND METHODS

The in vivo sheep model (2) consists of a transvalvularly placed transthoracic Hemopump Hp31 with its stiff metal housing being placed inside a graft. The inflow side of the Y-shaped graft is connected to the aorta ascendens and the outflow side to the aorta descendens thus diverting pump flow into the graft and back into the descending aorta. An electromagnetic flowmeter is integrated within the graft which is sealed around the stiff housing of the pump. Together with pressure measurements within the left ventricle and the aorta descendens, pump performance can be evaluated online. Pump speed is kept constant throughout the measurements.

Based on the in vivo results (2), 2 different in vitro set-ups have been designed, one with the pump inflow tip concentrically placed within a large tube and the other with it placed within an actively beating silicone ventricle. The reason for two test conditions is a two-step approach: perfect inflow conditions into the pump in the first case, and impaired inflow conditions in the second case caused by attachment of the inflow tip to the wall of the silicone ventricle and resulting suction.

The pulsatile mock loop is shown in Fig. 1 with optimum inflow conditions consisting of a chamber open to atmospheric pressure from which the fluid passes through a porcine valve into the pump. The pump inflow cannula is centered inside a large tube that is connected and sealed to a second pressure-sealed chamber, simulating the arterial system with air compliance. Within the backflow line, a systemic resistance and an ultrasound flowmeter are integrated (Model HT109; Transonic Systems, Inc., Ithaca, New York, U.S.A., with the Transonic flowprobe Model H11X1) to check the systemic flow. A pulsatile fluid actuator is integrated between the porcine valve and the sealed pump unit. Systolic ejection is linked directly to the motion of the actuated pusher plate whereas diastolic filling is passive because the membrane is not attached to the 60 cc displacing pusher plate. Consequently, diastolic filling of the device is based only on the geodetic difference of the inflow and outflow ports and the water levels between the actuator and the mock loop chambers. A second compliance within the fluid chamber of the pulsatile actuator levels out unphysiologic pressure peaks. This set-up is thought to provide optimum inflow conditions into the pump because the inflow tip of the cannula is located inside a large tube without any tip-to-wall contact. The porcine valve opens immediately

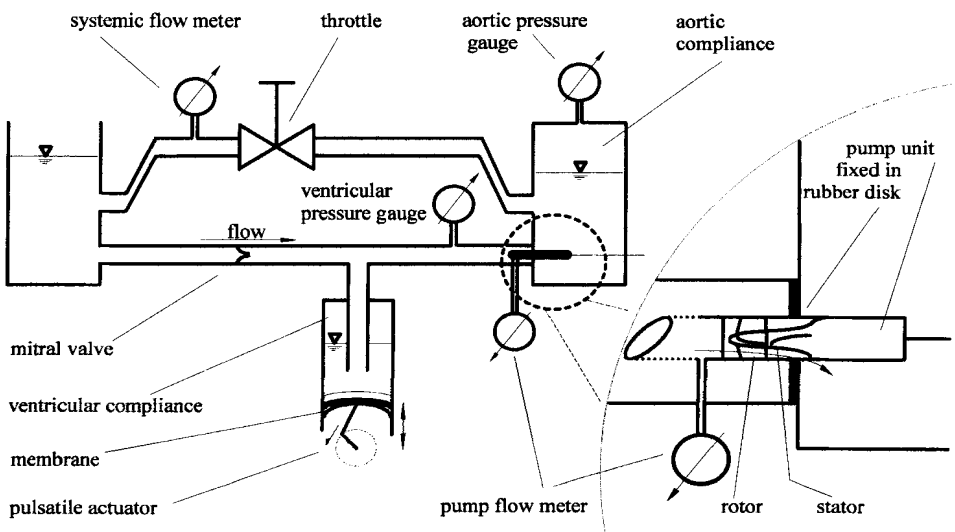


**FIG. 1.** A pulsatile mock loop is shown with the pump fixed and centered inside of a 25 mm tube resulting in optimum pump inflow conditions through a porcine valve in the mitral position from a venous reservoir.

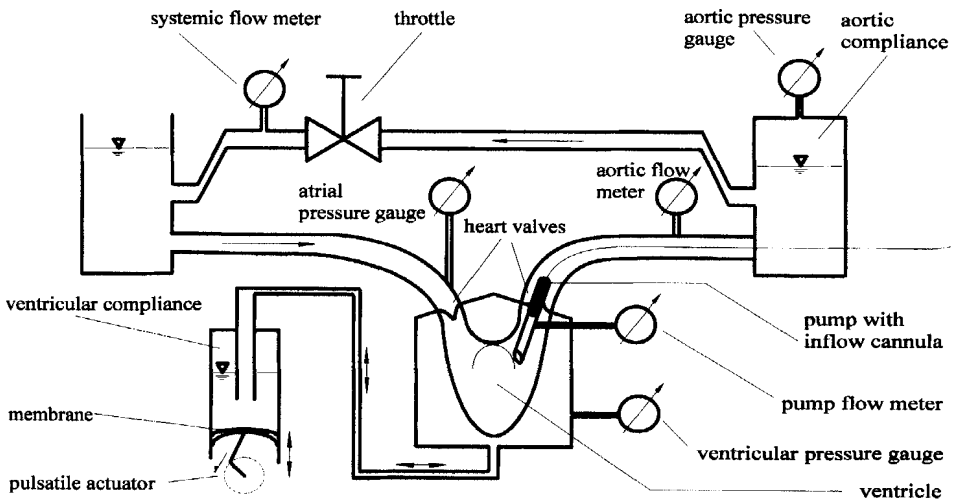


**FIG. 2.** A pulsatile mock loop is shown with an integrated beating silicone ventricle driven by a pulsatile actuator.

when the pressure within the simulated left ventricle decreases below atrial inflow pressure. In this case, fluid from the venous reservoir enters the ventricular line without any relevant resistance. The pressure difference across the pump is measured by 2 disposable pressure transducers (Cobe, Lakewood, Colorado, U.S.A.) located proximally to the pump inflow tip and within the pressure-sealed aortic chamber. Thus, taking the geodetic difference of the water levels between the 2 pressure transducers into account, the measured pressure represents the pressure difference across the pump. Pump flow is measured via an electromagnetic flowmeter with a 70-Hz lowpass (Zepeda Instruments, Seattle, Washington, U.S.A.) with a Ø7 mm (CA flow probe) which is located between the inflow cannula and the pump.

The second pulsatile set-up, shown in Fig. 2, is basically similar to the set-up described in Fig. 1, except for the integrated silicone ventricle. The thin, flexible ventricle is embedded inside a stiff Plexiglas casing as illustrated in Fig. 3, with porcine valves in the mitral as well as in the aortic positions and an additional port for the pulsatile actuator. The intravascular pump is located similarly to that in the in vivo model, in a transvalvular position. The flowmeter and pump are placed in the aorta ascendens as illustrated in Fig. 4. The three flexible leaflets of the aortic valve seal around the inflow cannula and minimize regurgitation during the diastolic filling phase. Because the silicone ventricle may eject fluid across the aortic valve during the peak systolic ejection phase, an aortic flowmeter (Zepeda Instru-

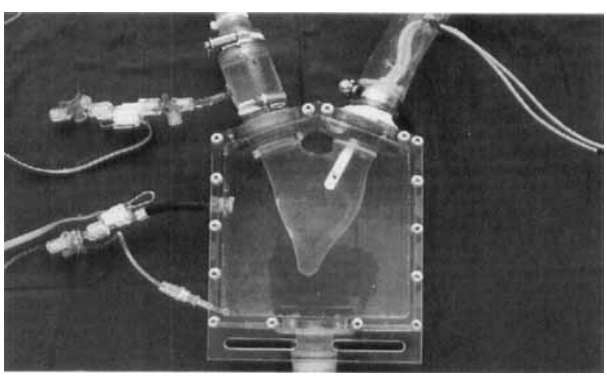

**FIG. 3.** A silicone ventricle within a rigid Plexiglas housing is shown. Two porcine valves are placed inside of the inflow and outflow ports. The port on the lower bottom connects the housing to the pulsatile actuator.

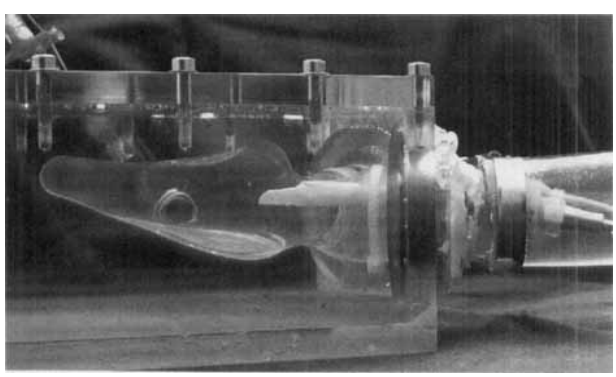

**FIG. 4.** The end-diastolic filling volume of the silicone ventricle is shown yielding good inflow conditions into the pump at all pump speeds. Although the tip of the pump is located in the center of the ventricle, the electromagnetic flowmeter and the housing of the pump are located outside the ventricle within the aortic line.

ments, Seattle, Washington, U.S.A. with Ø16-mm CA flow probe, 70 Hz lowpass) has been integrated to measure the resulting cardiac output summing up of the output of the ventricular and pump. In this set-up, ventricular pressure is measured with a disposable transducer (Cobe, Lakewood, Colorado, U.S.A.) at the level of the inflow tip within the stiff ventricular casing but outside of the silicone ventricle thus assuming that the driving pressure inside the casing and within the ventricle is equal as long as the silicone ventricle is not stretched during any period of the cardiac cycle. Consequently, the fluid and air volumes within the actuator system must be adjusted to an end-diastolic filling volume of the silicone ventricle, which results in a tension-free state within the silicone wall as illustrated in Fig. 4. For complete monitoring of the ventricular filling situation, a third pressure transducer has been integrated to measure the atrial pressure proximal to the mitral valve.

Experimental readings of the pump operation at different pump speeds with alternating ventricular pressures have been recorded on an IBM-compatible personnel computer using Labview software (National Instruments, Austin, Texas, U.S.A.). The sampling frequency was set to 1,000 Hz for each channel to obtain flow and pressure curves that include fairly accurate peak values. The collected data have been modified and processed using Microsoft Excel (Microsoft, Bellevue, Washington, U.S.A.).

## GOALS OF THE EXPERIMENT

First, the initial goal of the in vitro experiments was the validation of the experimental in vivo findings. At constant speed settings, the in vivo pressure flow loops during 1 cardiac cycle reveal that the pump flow does not move back and forth in a straight line as a function of the pressure difference but rather that it circles around in a loop with a distinct hysteresis. Figure 7 in Meyns et al. (2) illustrates that the width of the hysteresis is related to the pump speed resulting in wider loops and lower flow rates at pump Speed 1 than at Speed 7. Pulsatile pump performance measurements must be performed in both in vitro set-ups to verify these in vivo findings and to clarify the underlying mechanisms.

Second, despite the character of the cyclic loop of the pump, it must be discussed if the calculation of pump flow based on the pressure difference only can be applied to characterize the online in vivo pump flow without flow sensors.

Third, identification must be made of the mechanisms leading to a decrease in in vivo pump flow at Speed 7 compared with Speeds 5 and 6 in some sheep.

Fourth, a better understanding is required of the ventricle's interaction with a rotary nonpulsatile pump, and development of a more sophisticated pump management system must be undertaken.

## RESULTS

### With good inflow conditions into pump

Figure 5 shows a characteristic, dynamic, in vitro flow loop of the Hp31 running at Speed 1 and with the pulsatile actuator set at 70 bpm. The pressure flow loop moves clockwise which is characteristic for all loops obtained at good inflow conditions into the pump. Following the loop the aortic valve closes at $\Delta p = 0$ mm Hg and $\dot{V} \cong 3.3$ L/min with

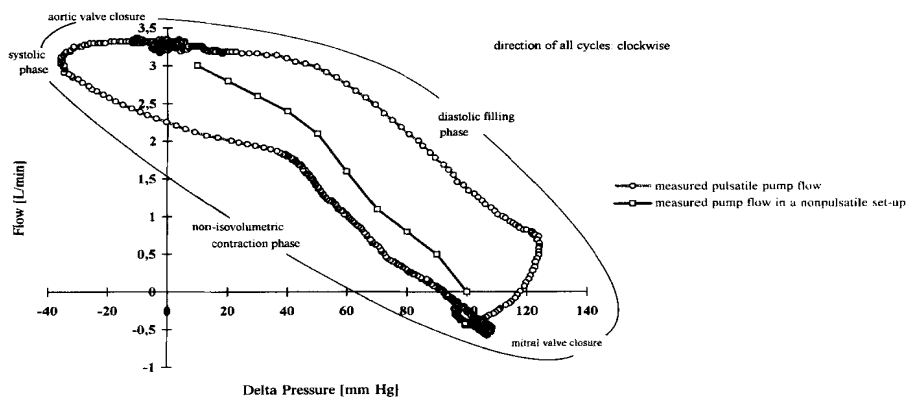


**FIG. 5.** An in vitro flow loop of the Hp31 during 1 cardiac cycle at 70 bpm is compared to the static flow curve at pump Speed 1 acquired from a nonpulsatile mock loop; the elapsed time between two consecutive dots on the pulsatile flow loop is 1/1000 s illustrating the velocity of different cyclic phases.

noticeable pressure peaks caused by the rigid set-up and the rapid deceleration of the fluid moving within the tubing and ventricle and leading to a small horizontal loop around $\Delta p = 0$ mm Hg. The closing phase of the aortic valve is followed by a rapid diastolic relaxation phase and, after opening the mitral valve, by a comparably long diastolic filling phase. Mitral valve closure is marked by a characteristic small loop at $\Delta p \cong 95$–110 mm Hg resulting from effects similar to those occurring during aortic valve closure. This phase is followed by the isovolumetric contraction phase. In this case, the isovolumetric contraction phase is not purely isovolumetric because of the active unloading of the pump and is unphysiologically long because of the sinusoidal movement of the pusher plate resulting in a rather slow displacement of fluid at the beginning of the systolic phase in conjunction with the continuously unloaded ventricle. As soon as the aortic valve opens at $\Delta p \cong 0$ mm Hg, the systolic ejection phase begins, and the silicone ventricle actively ejects fluid through the aortic valve parallel to the pump during the period of negative pressure difference. Then, the aortic valve closes again around the inflow cannula of the pump, and a new cycle begins.

Although this chart (Fig. 5) shows the pump flow as a function of pressure difference, the time span for each cyclic phase can be calculated qualitatively from the distance between two consecutive dots with the time span being 1/1,000 s. Long distances between two dots consequently mark a rapid change in flow or pressure.

Interpretation of measurements with the pump at zero rotation speed up to Speed 7 with beat rates of 40, 55, and 70 in both in vitro set-ups led to the conclusion that optimum inflow conditions can be obtained equally within the two experimental in vitro set-ups. As long as the end-diastolic volume of the silicone ventricle is sufficiently large (such as that shown in Fig. 4), the difference in results between each set-up is negligible. Consequently, only results with the second set-up, which used the silicone ventricle, are illustrated and discussed below.

For comparison, Fig. 6 shows the Hp31 performance with the silicone ventricle at a beat rate of 70 bpm at pump Speeds 1, 4, and 7. Analog to the in vivo findings in Fig. 7 in Meyns et al. (2), the pump produces characteristic flow loops in vitro with a similar rotational speed dependency. The width of the hysteresis is reduced and the flow enhanced with increasing pump speed as described earlier for the in vivo results. Differences in measured pressure differences during a cardiac cycle result from the fact that the peripheral resistance as well as the vascular elasticity and compliance in vivo cannot equally be simulated in vitro with this fairly simple set-up. Furthermore, heart activity which is based on numerous factors such as contractility and end-diastolic filling volume cannot be simulated by the sinusoidal movement of the pusher plate with a fixed stroke volume and only one compliance chamber inside of the actuator. Both simplifications lead to a significantly higher range of pressure differences in vitro with even negative pressures of up to −45 mm Hg, meaning that in vitro the peak systolic ventricular pressure exceeds the measured aortic pressure within the sealed reservoir by 45 mm Hg because of fluid inertia effects and comparably stiff tubing between the aortic valve and the reservoir. Despite the visible difference in the in vivo mea-

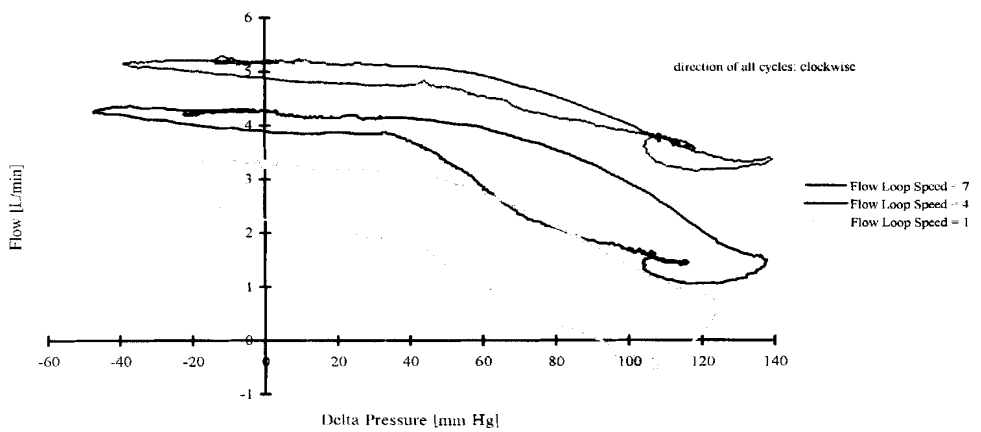


**FIG. 6.** In vitro flow loops of the Hp31 at speeds 1, 4, and 7 show significantly different widths of hysteresis and pump performance at different pump speeds under optimum inflow conditions.

surements, the same effects can be demonstrated qualitatively in vitro.

To find a suitable explanation for the characteristic flow loops of a high frequency pump which rotates with up to 430 Hz at 26,000 rpm (≅Speed 7), it appears to be difficult to determine that changing flow patterns within the pump are responsible for the visible hysteresis. In a first approximation, global physiological pressure changes during 1 cardiac cycle are quasi stationary changes for the high-frequency pump.

One suitable explanation of the hysteresis is certainly the influence of inertia on pump behavior in a pulsatile environment: The difference between the pulsatile or nonpulsatile mode is a force component derived from the accelerated and decelerated mass within the pump and cannula:

$$F = \frac{d}{dt}(m \times \mathrm{v}) = \frac{\delta m}{\partial t} \cdot \mathrm{v} + \frac{\delta \mathrm{v}}{\partial t} \cdot m = \frac{d\mathrm{v}}{dt} \cdot m \quad (1)$$

(incompressible fluid, m = const.)

The relevant quantity needed to characterize the difference between pulsatile and nonpulsatile pump behavior is the additional differential pressure $\Delta P'$ over the pump which results from the force $F$ (Eq. 1) divided by the relevant area which is equal to the cross section area $A$ of the cannula with the mass $m$ being the fluid within the pump and cannula:

$$\Delta P' = \frac{F}{A} = \frac{1}{A} \cdot \frac{d\mathrm{v}}{dt} \cdot m = L \cdot \frac{\rho}{A} \cdot \frac{d\dot{V}}{dt} \cong L \cdot \frac{\rho}{A} \cdot \frac{\dot{V}(t_i + \Delta t) - \dot{V}(t_i)}{\Delta t} \quad (2)$$

where v is the fluid velocity within the cannula; $m$ is the mass within the cannula and pump; $L$ is the length of the cannula; $\rho$ is the fluid density; $A$ is the cross-section area of the cannula and pump; $\dot{V}$ is the volume flow; $t_i$ is the specific time step; and $\Delta t$ is the elapsed time between specific time steps. The measured $\Delta P$ over the pump derived from the aortic pressure minus the ventricular pressure modified by $\Delta P'$ should yield a reduced hysteresis within the $\Delta P - \dot{V}$ diagram of the pump.

Figure 7 illustrates a regular pulsatile flow loop (in black) of the Hemopump at Speed 4 and a pulsatile flow loop which has been normalized with the fluid inertia $\Delta P - \Delta P'$ within the pump and cannula (light grey). This normalized loop can be interpreted as a corresponding loop for a pump without an inflow cannula. For comparison purposes, the in vitro nonpulsatile measurement of the pump at Speed 4 is integrated (dark grey) to demonstrate that the pulsatile flow loops basically circle around the nonpulsatile control measurements.

Comparing both pulsatile loops shows that the width of the hysteresis is reduced considerably by subtracting the impact of fluid inertia on pump performance leading to a narrow loop which comes close enough to a line. This fairly simple first approximation also can explain the significantly higher hysteresis measured in vivo compared with the in vitro findings. This difference simply results from diverting the pump flow around the aortic arch within a graft in vivo. This graft behaves like an elongated outflow cannula because it is rather stiff due to the arterial pressure that keeps the graft inflated. Thus, the relevant fluid mass in vivo is considerably higher than that seen in vitro resulting in a higher hysteresis. Despite the fact that the flow pat-

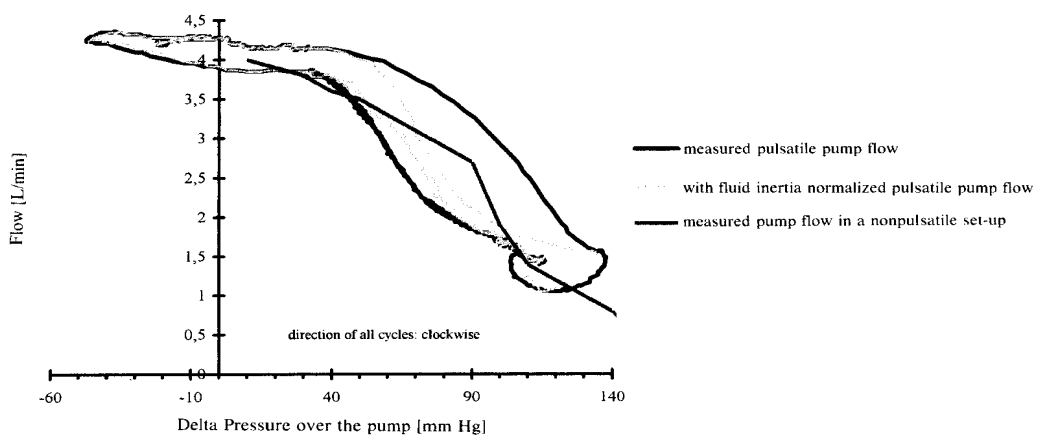


**FIG. 7.** An in vitro flow loop of the Hp31 at Speed 4 is compared with a measured control nonpulsatile flow curve and a pulsatile flow loop with reduced hysteresis achieved by the elimination of the impact of fluid inertia within the pump and cannula.

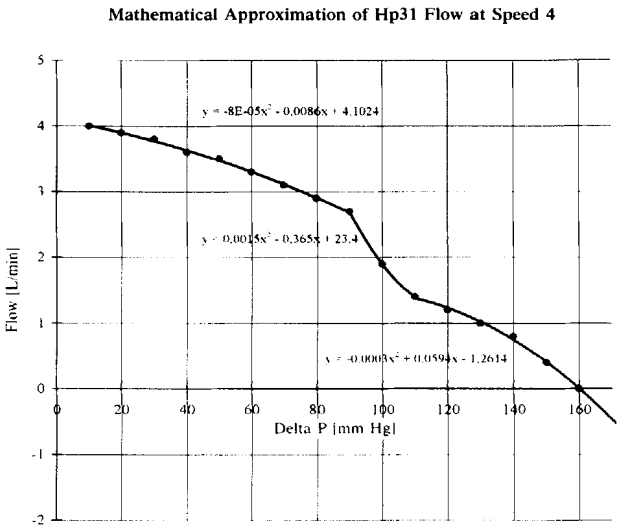


**FIG. 8.** An in vitro nonpulsatile flow curve of the Hp31 at Speed 4 is approximated mathematically for characterization of the pump flow as a function of the pressure difference.

tern inside the pump also contributes to the hysteresis loop, the impact of fluid mass inertia on pump performance may be sufficient to explain the hysteresis phenomenon in this first approximation so that further investigations of a useful characterization of the pump-ventricle interaction are not necessary.

Realizing that the pulsatile flow loop of the pump circles around the nonpulsatile control measurements for all pump speeds, it appears useful to calculate the pulsatile pump flow as a function of the pressure difference based on the nonpulsatile control pump flow measurements. To obtain a mathematical correlation of pump flow based on these measurements, the nonpulsatile flow curves of the pump have been approximated mathematically as illustrated in Figs. 8 and 9 for pump speeds 4 and 7, respectively. According to these correlations, the corresponding flow has been calculated based on the measured in vitro pressure differences. Figures 10 and 11 show the results for the Hp31 at Speeds 4 and 7, respectively, illustrating that the calculated pump flow nicely matches the in vitro measured pulsatile pump flow. Visible differences between the measured and calculated flows result from the hysteresis and mass inertia impact, respectively, as discussed previously. Thus, lower hysteresis at Speed 7 leads to a better correspondence of flow than at Speed 4 (as illustrated in Fig. 11 compared to 10). Comparison of the curves reveals that the measured flow curve leaps behind the calculated curve and also filters the pressure peaks caused by the influence of fluid inertia.

Despite these minor differences, one can conclude that a pressure difference across the pump and a mathematical function of the pump flow obtained from nonpulsatile in vitro measurements may result in a useful calculated pump flow without the need for online pump flow measurements as long as a sufficient blood supply is available during the cardiac cycle and inflow into the pump is not impaired.

## RESULTS

### With impaired inflow conditions into pump

Figure 12 illustrates Hp31 performance in a 67 kg male sheep with a rather small ventricular cavity.

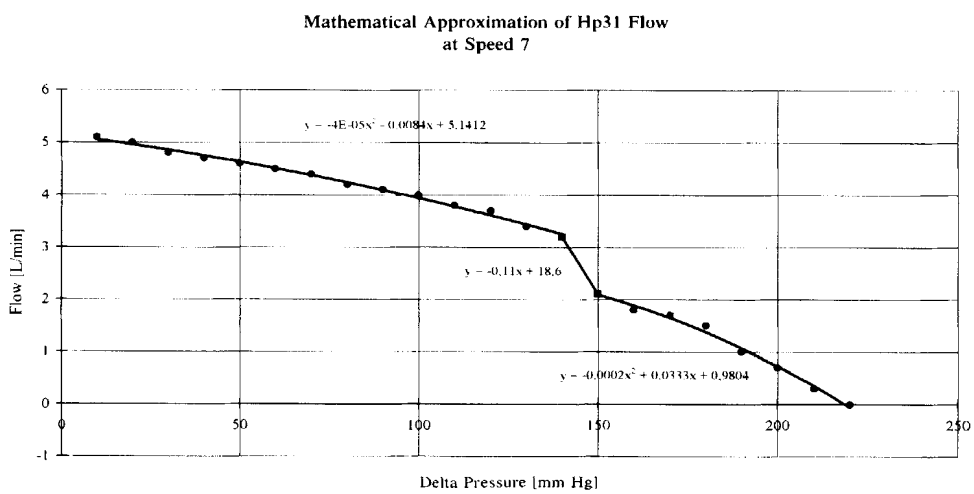


**FIG. 9.** An in vitro nonpulsatile flow curve of the Hp31 at Speed 7 is approximated mathematically for characterization of the pump flow as a function of the pressure difference.

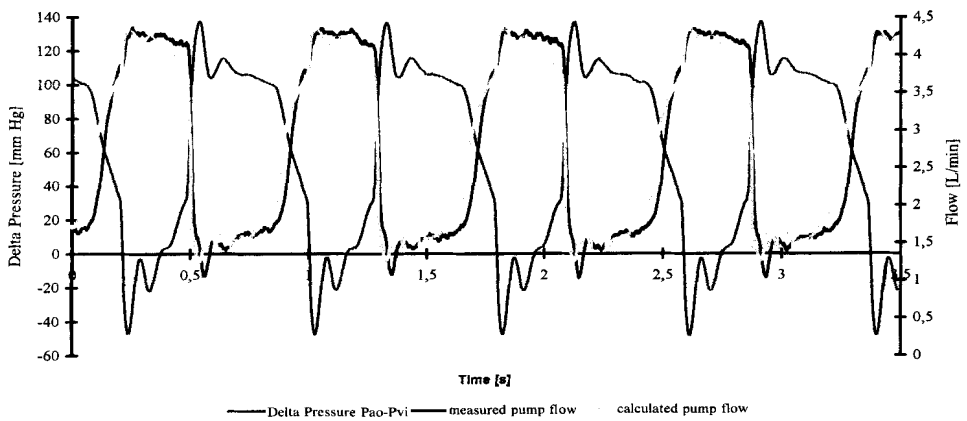


**FIG. 10.** A measured pump flow is compared to the calculated pump flow as a function of the pressure difference at Speed 4 under optimum inflow conditions.

Although mean pump flow could be increased considerably, from Speed 3 to Speed 6, it dropped down at Speed 7 to the levels seen at Speed 4. Arrhythmia occurred randomly at Speed 6 and continuously at Speed 7 revealing that the unloading of the ventricle leads to a small cavity at Speed 6 with arrhythmia caused by randomized tip-to-wall contact. At Speed 7, arrhythmia occurred regularly with a ventricular size referred to being "overunloaded" with more frequent tip-to-wall contact. Corresponding to a shrinking ventricle, the left ventricular peak pressure decreased from 100 mm Hg to only 50 mm Hg at Speed 7.

Figure 8 from Meyns et al. (2) illustrates a corresponding pump flow loop during 1 cardiac cycle in vivo at Speed 7 with impaired inflow. Whereas a regular flow loop under good inflow conditions moves clockwise, this loop moves counterclockwise. At peak systolic flow conditions of 3.8 L/min and a pressure difference of 35 mm Hg, the flow decreases to 2.3 L/min because of impaired inflow; and circles back to an end-diastolic pressure difference of 75 mm Hg at 3 L/min followed by a fairly normal flat flow phase during the nonisovolumetric filling and systolic ejection phase of the ventricle. According to this figure, impaired inflow occurs mostly during the end-systolic ejection and diastolic filling phases of the ventricle.

These in vivo findings have been simulated in vitro to relate momentary ventricular shapes and sizes to corresponding pump flows. Whereas the end-diastolic ventricular shape in Fig. 4 shows good inflow conditions into the pump, Fig. 13 illustrates a completely unloaded and therefore collapsed ventricle at the end of the peak systolic phase leading to tip-to-wall contact that causes local suction and arrhythmia in vivo. Consequently, as described above, pump flow in vivo decreases immediately

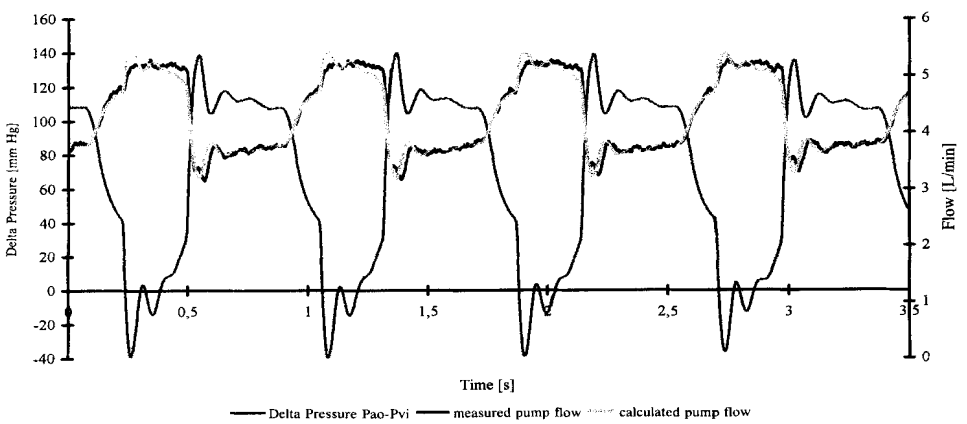


**FIG. 11.** A measured pump flow is compared to the calculated pump flow as a function of the pressure difference at Speed 7 under optimum inflow conditions.

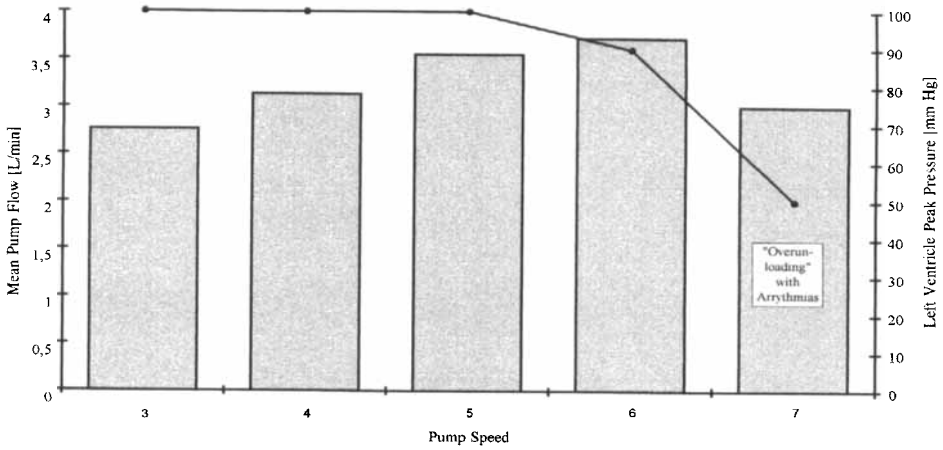


**FIG. 12.** Pump flow in a 67 kg male sheep with a small left ventricular cavity leads to impaired inflow conditions especially at higher pump speeds. Impaired inflow or a low blood supply can be further related to a decrease in left ventricular peak pressures as illustrated.

after the peak systolic phase with somehow similar inflow conditions into the pump (illustrated in Fig. 13), and remains comparably low. Figures 14 through 16 show corresponding flow loops in vitro at pump Speeds 1, 4, and 7 during impaired inflow conditions that result from partial clamping of the atrial line. Corresponding to the in vivo results shown in Fig. 12, impaired inflow is less obvious at lower pump speeds. At Speed 1 the resulting clockwise loop still moves closely around the corresponding nonpulsatile control flow curve whereas at Speed 4 the loop already drifts out of the control situation. At Speed 7 the pump flow remains considerably below the control curve, and no longer moves in a clockwise loop. The resulting in vitro loop has the shape of a lying 8 and can be compared with the more drastic counterclockwise loop in vivo.

Whereas in vivo the pump flow (Fig. 8 [2]) decreases immediately after the peak systolic phase, the flow in vitro decreases more slowly, crossing over Part 1 of the flow curve during the diastolic filling phase. Thus, one can conclude that inflow obstruction into the pump in vivo is even more severe than in this first in vitro simulation.

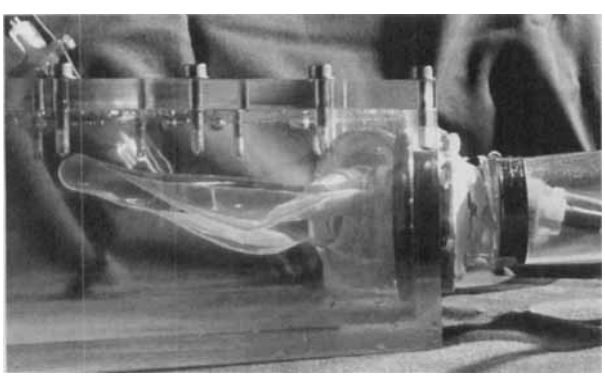

**FIG. 13.** This photograph shows a totally collapsed ventricle during the end-systolic phase, leading to temporary total obstruction of the inflow cannula and zero pump flow.

Consequently, further dynamic unloading experiments achieved by injecting 80 cc of water into the circuit of the pulsatile actuator have been performed leading to the end-systolic ventricular shapes seen in Fig. 13, which shows a fully collapsed ventricle. Fig. 17 shows the dynamic process of actively unloading the ventricle up to a shape similar to that in Fig. 13. Beginning with good inflow conditions, Loop 1 consequently moves around the control Hp31 flow at Speed 7. During the active unloading process via volume injection into the circuit of the pulsatile actuator, the consecutive loops show a drastic decrease in pump flow circling down from Loop 1 to Loop 10 with Loop 10 being at the bottom of the chart and showing peak flows of only 1.7 L/min during the first half of the nonisovolumetric contraction phase. Similar to the in vivo findings for severely impaired inflow conditions, all of the in vitro loops move counterclockwise. The obvious unphysiological shift to negative pressure differences during the unloading process is one trade-off of this rather simple in vitro set-up. Whereas ventricular pressures in vivo are likely to decrease with shrinking ventricular cavities because of the Frank-Starling mechanism, the contractility of the pulsatile actuator remains constant during the active unloading phase, which leads to unphysiologically high systolic ventricular pres-

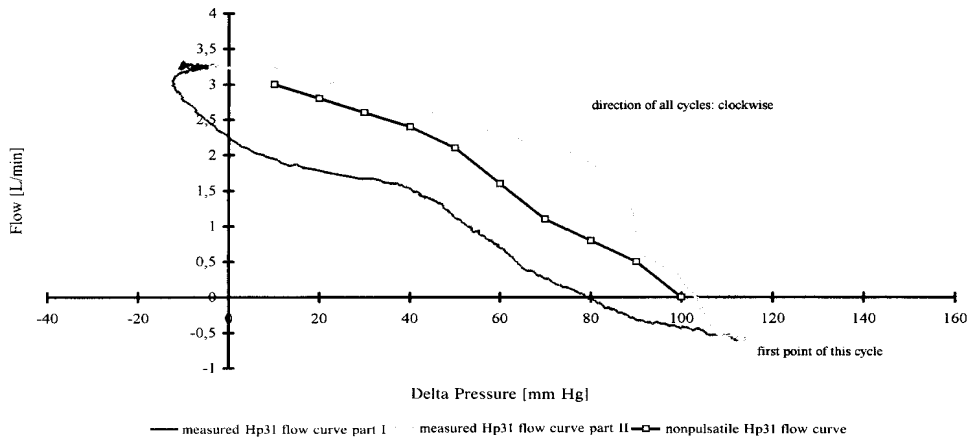


**FIG. 14.** Induced impaired inflow into the pump caused by inhibited ventricular inflow conditions simulated by partially clamping the atrial line at pump Speed 1 is compared to a nonpulsatile control curve of Hemopump flow. Impaired inflow does not reduce pump performance significantly because the loop still moves around the control curve.

sures especially for small residual ventricular volumes.

Figure 18 illustrates the same results of the measured pump flow based on a time scale. Included in this chart is the momentary pressure difference across the pump and a calculated pump flow based on the measured pressure difference and the mathematically approximated nonpulsatile control flow curve at Speed 7. Unlike in Figs. 10 and 11, the calculated pump flow increases while the measured flow decreases during consecutive cycles. Consequently, the calculated pump flow can no longer serve as a reliable pump performance indicator when inflow conditions are impaired. According to in vivo left ventricular pressure readings, impaired inflow into the pump never resulted in negative ventricular pressures indicating that suction leading to lower pump flows occurs locally at the tip and cannot be measured via a pressure transducer inside the ventricular cavity.

## CONCLUSIONS

Based on these in vivo and in vitro experiments, one can conclude that a calculated pump flow based on pressure difference measurements of aortic pressure minus ventricular pressure may be a reasonable pump performance indicator when good pump filling is secured. This is only the case when the pump is operating in a dilated left ventricle with sufficient blood supply coming from the right side. In other cases, impaired inflow may occur as a con-

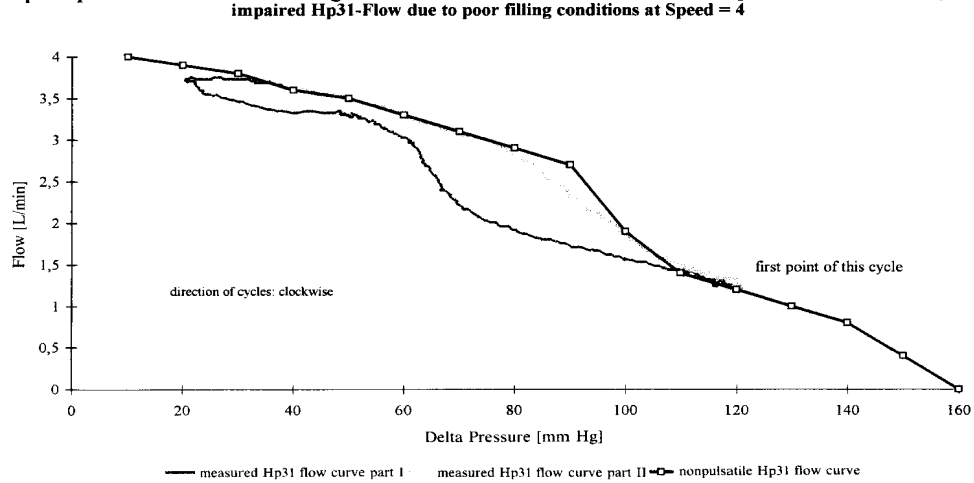


**FIG. 15.** Induced impaired inflow into the pump caused by inhibited ventricular inflow conditions by partially clamping the atrial line at pump Speed 4 is compared with a nonpulsatile control curve of Hemopump flow. Impaired inflow reduces pump performance because the loop moves below the control curve.

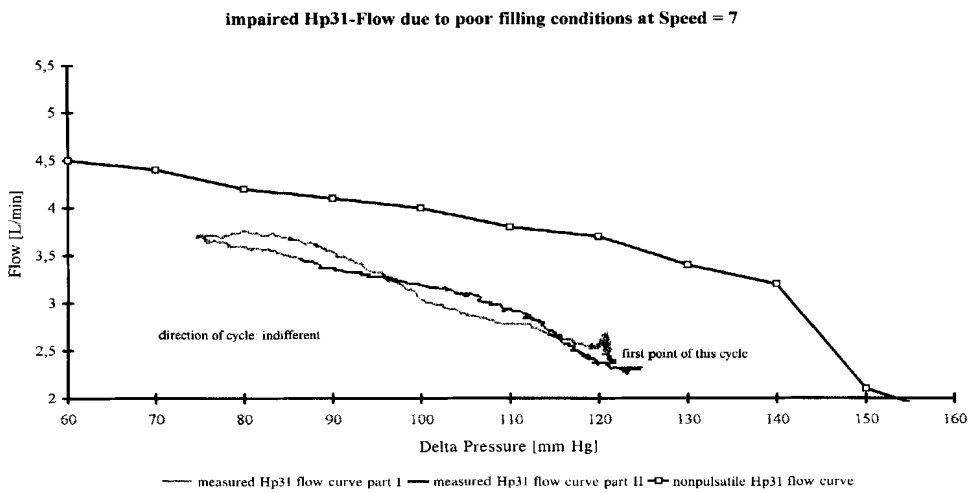


**FIG. 16.** Induced impaired inflow into the pump because of inhibited ventricular inflow conditions simulated by partially clamping the atrial line at pump Speed 7 is compared with a nonpulsatile control curve of Hemopump flow. Impaired inflow significantly reduces pump performance resulting in an indifferent flow loop.

sequence of tip-to-wall contact or insufficient filling so that the calculated pump flow can be misleading as illustrated in Fig. 18. According to Fig. 12, pump flow may even be higher at lower pump speeds compared with Speed 7 because of better filling and inflow conditions into the pump. Therefore, a patient with low cardiac output and the pump running at Speed 7 might do better at lower pump speeds. Lower speed may be more desirable to achieve a higher total cardiac output.

Considering these findings, further investigations of a measured pressure difference in conjunction with a measured motor current must be conducted to find a reliable indicator of pump performance. The integration of any kind of flow or velocity sensor within the pump cannula appears to be the most desirable solution, but it is costly and requires an extremely small and durable sensor.

Further utilization of the motor current signal of the extracorporeal pump driver of the Hemopump system for exact calculations of pump power demand and flow is difficult because the flexible drive shaft contributes significant friction losses.

For the development of the Helmholtz intravascular pump with the integrated drive unit proximal to the pump unit, the use of the motor current signal is easier because the pump impeller is connected directly to the motor leading to a power related current signal that can be used directly to characterize the pump flow. This may be possible if the impeller

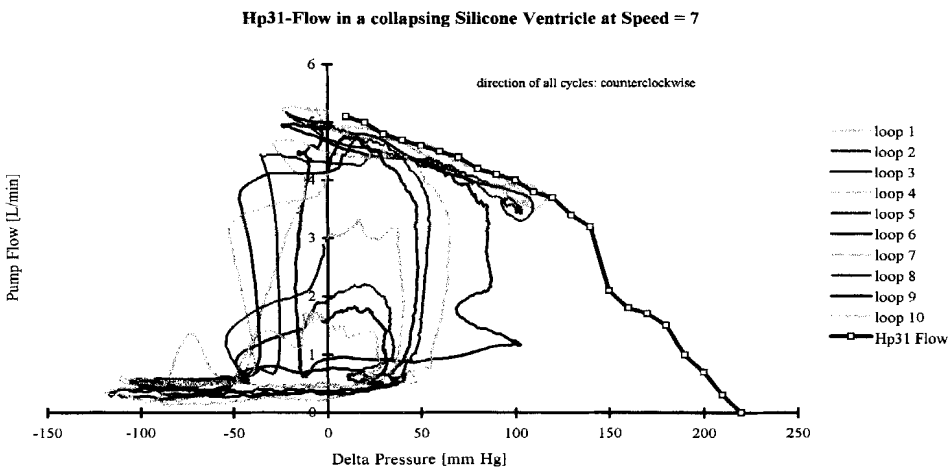


**FIG. 17.** Consecutive flow loops of the Hp31 at Speed 7 are shown with the ventricle being unloaded actively down to an end-systolically collapsed ventricle.

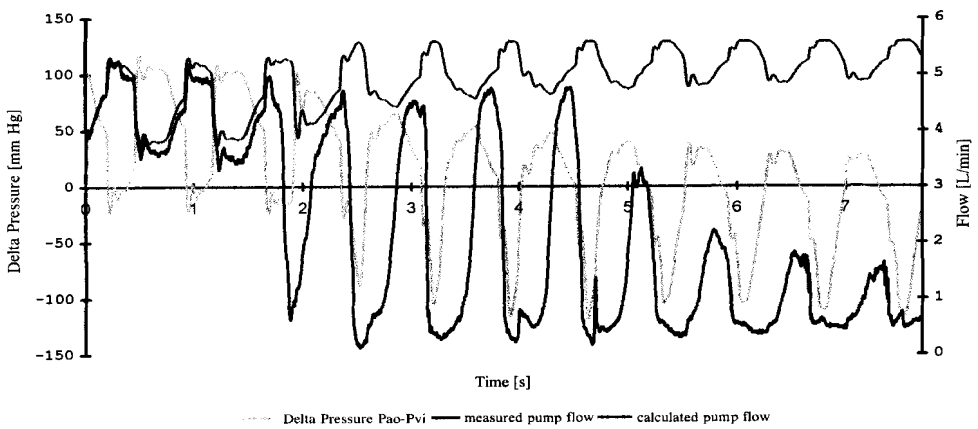


**FIG. 18.** Flow and pressure curves of the Hp31 at Speed 7 with the ventricle being unloaded actively down to an end-systolically collapsed ventricle are compared to a calculated pump flow based on a mathematical approximation.

design shows a characteristic power-flow relationship based on flow and pressure head at a specific at a specific rotation speed.

Ongoing investigations will determine if a simple system without additional sensors can serve as a reliable pump performance indicator even in cases of pump obstruction due to thrombus deposits.

## REFERENCES

1. Waldenberger FR, Wouters P, Wiebalck A, Flameng W. Use of the left-ventricular assist with the Hemopump in cardiac surgery. *Cardiology* 1994;84:211–5.
2. Meyns B, Siess T, Laycock S, Reul H, Rau G, Flameng W. The heart-Hemopump Interaction: a study of Hemopump flow in function of cardiac activity. *Artif Organs* 1996;20(6): 000–000.
3. Mees U, Sergeant P, Daenen W, Flameng W. *Success and failure of the Hemopump: a critical analysis.* New York: Steinkopff Verlag Darmstadt/Springer-Verlag, 1991.
4. Kunst E, van Alsté J. Dynamic pumping characteristic of the Hemopump—a small intraventricular bloodpump. *Proceedings of the International Workshop on Rotary Blood Pumps*, Vienna, 1991.
5. *Hemopump cardiac assist system: directions for use.* Rancho Cordova, CA: Johnson & Johnson Interventional Systems Co.
6. Siess T, Reul H, Rau G. Concept, realization, and first in vitro testing of an intraarterial microaxial blood pump. *Artif Organs* 1995;19(7):644–52.
7. Siess T, Reul H, Rau G. Hydraulic refinement of an intraarterial microaxial blood pump. *Int J Artif Organs* 1995;18(5): 27 3–85.